Polymorph Analysis of ALZ-801 (Valiltramiprosate), a Valine-conjugated Oral Prodrug of Tramiprosate in Late-stage Clinical Development for Alzheimer's Disease

D. Pearson
Sygnature Discovery (United Kingdom)
J. Amedio
Alzheon, Inc
J. F. Schaefer
Alzheon, Inc
M. Tolar
Alzheon, Inc
John A. Hey
John.Hey@Alzheon.com

Alzheon, Inc

Research Article

Keywords: Polymorphism, crystal structure, ALZ-801, tramiprosate, prodrug

Posted Date: December 23rd, 2024

DOI: https://doi.org/10.21203/rs.3.rs-5580809/v1

Additional Declarations: Competing interest reported. Funding support: The analyses in this report were supported by Alzheon, Inc. Conflicts of interest: John A. Hey, Jean F. Schaefer, and Martin Tolar are employees of Alzheon, Inc. John Amedio, serves as a consultant to Alzheon, Inc. All authors own Alzheon stocks and/or stock options. David Pearson is an employee of Sygnature Discovery. Availability of data and material: The ALZ-801 data are proprietary to Alzheon Inc.

Abstract

ALZ-801 (valiltramiprosate) is an orally bioavailable, small-molecule inhibitor of β-amyloid (Aβ) oligomer formation in late-stage clinical development as a potential disease-modifying treatment for Alzheimer's disease (AD). ALZ-801, (S)-3-(2-amino-3-methylbutanamido) propane-1-sulfonic acid, is a valine-conjugated prodrug of tramiprosate. Structural, polymorphic analysis of the active pharmaceutical ingredient (API) of ALZ-801 showed extra peaks when high throughput transmission mode XRPD analysis was utilized. After extensive investigation, the extra peaks were determined to be an artifact of transmission mode XRPD, which was not observed in either reflectance or capillary mode XRPD analyses. Reflectance mode XRPD was demonstrated as the most appropriate methodology to monitor the crystal form of ALZ-801 API. In conclusion, ALZ-801 API is a single polymorph form.

Introduction

One of the hallmark pathologies in Alzheimer's disease (AD) is the deposition of aggregated amyloid-beta (Aß) in the extracellular space of affected brains. A substantial body of scientific evidence, including genetic studies of familial AD, genome wide association studies, and biomarker studies in both familial and sporadic AD, supports the role of misfolded Aß monomers into oligomers as early drivers in AD pathogenesis [1, 2]. As the misfolding and subsequent aggregation of Aß monomers into oligomers overwhelms the brain's clearance mechanisms, these toxic soluble oligomers adopt prion-like capabilities that seed aggregation and propagation to neighboring brain structures [1, 3], triggering downstream cascades that ultimately lead to neurodegeneration and AD progression.

ALZ-801/valiltramiprosate (Fig. 1) is a novel small molecule oral agent composed of tramiprosate, the active agent, conjugated to the amino acid valine. Tramiprosate was developed as an Aβ anti-aggregation agent, with positive effects in both in vitro and in vivo models of AD [4]. In recent studies, tramiprosate showed dose-dependent inhibition of oligomer formation from dimers to dodecamers in vitro, mediated by electrostatic interactions between the drug and Aβ monomers that stabilize monomer conformation and inhibit their misfolding and aggregation into toxic oligomers [5, 6, 7].

ALZ-801 has been administered in human clinical trials and displayed promising efficacy in a Phase 2 study in early AD (7,8). ALZ-801 has been studied as an investigational product in both gelatin capsules with no excipients in Phase 1 studies [6] and as tablets with excipients in the Phase 2 [8, 9] and Phase 3 studies as an immediate release formulation for oral administration [10, 11, 12].

Figure 1: *Chemical structure of ALZ-801 and tramiprosate*

Analysis of the solid form of a material was performed to assess the crystal form using a variety of spectroscopy techniques such as ss-NMR [13], FT-IR [14] and Raman and NIR [15]. The gold standard for solid form analysis is single crystal x-ray diffraction [16]. However, this only analyzes a small portion of the material and as such evidence must be gathered that shows the single crystal is representative of the bulk material. The analysis of the bulk material using x-rays is performed by X-Ray Powder Diffraction

(XRPD), which is considered the industry standard tool to analyze the crystalline nature of a material. XRPD, however, does suffer from some drawbacks as it provides no information on:

1. Phase purity of the material, it could for example be a mixture of various forms which have not yet reached equilibrium;
2. Important characteristics of the sample; it does not for example tell you if it is a solvate, hydrate, degradant, or a salt of the material; and
3. Relative thermodynamic stability of the crystal forms being examined.

Although XRPD has these known caveats, it offers a critical advantage over other techniques in identifying whether a sample is crystalline. As such, it is widely accepted as the first line of analysis in the examination of solid form properties of a material.

Experimental

ALZ-801was received from Alzheon, Inc. (Framingham, MA). All solvents used in these studies were purchased from Fisher Scientific (Hampton, NH) and HPLC grade.

Transmission Mode XRPD

Transmission mode XRPD analysis was carried out on a PANalytical X'pert Pro with PIXcel Materials Research Diffractometer (128 channels; Malvern Panalytical, Malvern, UK), scanning the samples between 3 and 35° 2θ. The material was loaded into a multi-well plate with Kapton or Mylar polymer film to support samples. The multi-well plate was then placed into the diffractometer and the samples were analyzed using Cu K radiation (α1 λ = 1.54060 Å; α2 = 1.54443 Å; β = 1.39225 Å; α1 : α2 ratio = 0.5) running in transmission mode (step size 0.0130° 2θ, step time 18.87s) using 40 kV / 40mA generator settings.

Reflectance Mode XRPD

Reflectance mode XRPD analysis was carried out on a Philips X'Pert Pro Multipurpose diffractometer (Malvern Panalytical, Malvern, UK) equipped with a spinning stage. The samples were scanned between 4 and 35.99 °2θ using Cu K radiation (α1 λ = 1.54060 Å; α2 = 1.54443 Å; β = 1.39225 Å; α1 : α2 ratio = 0.5) running in Bragg- Brentano geometry (step size 0.008 °2θ) using 40 kV / 40 mA generator settings.

Capillary Mode XRPD

Capillary mode XRPD analysis was carried out on a Bruker D8 Venture

diffractometer with a Proton III C14 CPAD area detector (14x10; Bruker, Billerica, MA) and an Incoatec (Geesthacht, Germany) Cu IμS 3.0 monochromatic Kα (1.5418 Å) micro source operating at 50kV and

1.10mA. The sample was packed into a 0.5mm capillary and mounted onto the goniometer. The sample was optically aligned on the instrument so that during the phi scan the sample remained in the beam. A series of 120 second 360 ° phi scans (usually 14) at various 2θ values in both positive and negative scan directions were collected and then merged in the integration process using the Bruker Apex3 software (Version 2019.11-0).

Thermogravimetric/Differential Thermal Analysis (TG/DSC)

Approximately 5–10 mg of material was added into a pre-tared, open aluminum pan and loaded into a TA Instruments Discovery SDT 650 (TA Instruments, New Castle, DE) Auto - Simultaneous DSC and held at room temperature. The sample was then heated at a rate of 10°C/min from 30°C to 400°C during which time the change in sample weight was recorded along with the heat flow response (DSC). Nitrogen was used as the sample purge gas, at a flow rate of 200 cm3/min. TRIOS software (TA Instruments)

was used to analyze the data.

Differential Scanning Calorimetry (DSC)

DSC analyses were performed on a TA Instrument DSC250 with a Tzero cell purged at constant flow rate of 50 ml min^{-1} with dry nitrogen and a refrigerated cooling system RCS90. The instrument was calibrated using indium as a standard. A small quantity of the samples was put into TA Tzero Aluminum pan with a pierced lid. Samples were heated at 10°C/min in a heat-cool-reheat method. TRIOS software was used to analyze the data.

Nuclear Magnetic Resonance (NMR)

NMR experiments were performed on a Bruker AVIIIHD spectrometer equipped with a DCH cryoprobe operating at 500.12MHz for protons. Experiments were performed in deuterium oxide and each sample was prepared to ca. 10 mM concentration.

Results and Discussion

Polymorphism screen design and findings with ALZ-801

ALZ-801 is an API in late-stage clinical development and, while its high aqueous solubility would indicate that any change in polymorphic form affecting the performance of the drug product is small, understanding the crystalline landscape with subsequent control is an important pharmaceutical property and regulatory requirement.

When designing a polymorphic screen, the aim is to identify as many crystal forms as possible, not just the most stable form. Starting with amorphous material is preferred. If seeds of a crystal form that is

stable, or at least in a thermodynamic sink are present, they will prevent the formation of a crystal form which is higher in energy.

The formation of solvates was also investigated. Although rarely a developable form, solvates can offer a route to improve purity and aid in the isolation of a compound. They can also guide the selection of process solvents if a solvate needs to be avoided.

Initial analysis of ALZ-801 showed it to be highly crystalline and was designated as Pattern 1. Phase light microscopy revealed the crystal forms occur in a diverse range of morphologies, i.e., tetrahedron, bladed, needles, dodecahedron, slices, prismatic and tabular forms (Fig. 2). Preferred orientation as suspected, and a small sample was ground and analyzed again by transmission XRPD. The large particle size observed in many samples led to this assumption, as shown by the image of a crystal in Fig. 2 showing a crystal > 600 microns in length and 250 microns in width.

Figure 2: *Phase light microscopy image of ALZ-801 crystal pattern 1 (single polymorph). ALZ-801 crystals occur in diverse ranges of morphologies, i.e., tetrahedron, bladed, needles, dodecahedron, slices, prismatic and tabular forms.*

The two diffractograms are shown in Fig. 3.

Figure 3: *Transmission mode XRPD Diffractogram of ALZ-801 as received and after grinding.*

Thermal analysis showed good thermal stability with what looks like a melt decomposition observed at 329°C in the DSC. Weight loss occurs before this endothermic event, indicating degradation has already started. The TGA/DSC thermogram is shown in Fig. 4 and with the DSC thermogram in Fig. 5.

Figure 4: *TGA/DSC Thermogram of ALZ-801 as received.*

Figure 5: *DSC Thermogram of ALZ-801 as received.*

Attempts to render ALZ-801 by lyophilization were unachievable, as only crystalline material was returned as shown by the XRPD post-lyophilization (see Fig. 6).

Figure 6: *Transmission XRPD Diffractogram of ALZ-801 pre and post lyophilization.*

Spray drying, another technique available to render material amorphous, was not evaluated due to the high aqueous solubility of ALZ-801.

With only crystalline material available, the screen for alternative polymorphic forms was modified to allow other forms to be produced. Starting with a solution of ALZ-801 in various solvents, with no seeds of the pattern 1 present, the formation of different crystal forms was attempted. Evaporation at ambient temperature and pressure, rapid evaporation at elevated temperature, reverse anti-solvent addition, and crash cooling were all investigated. The high solubility of ALZ-801 resulted in the finding that experiments conducted did not yield solids for analysis. There were, however, solids produced which

allowed investigations into the solid state of ALZ-801. Many of the samples analyzed showed preferred orientation effects. Examples of diffractograms form various experiments are shown in Fig. 7 with an expansion in Fig. 8.

Figure 7: *Transmission mode XRPD diffractograms from selected experiments.*

Figure 8: *Expansion of transmission mode XRPD diffractograms from selected experiments.*

Preferred Orientation and Further Analysis

During the analysis of solids preferred orientation and/or extra peaks were observed in the transmission mode XRPD diffractograms as exemplified in Fig. 8. Additional experiments allowed investigation of the extra peaks/preferred orientation in more detail. Material was produced in both methanol as well as a THF-water mixture. The sample from methanol was analyzed by TGA/DSC, DSC and ^{1}H NMR initially and the analysis was repeated following a gentle grinding using a pestle and mortar. The resulting ground material was also analyzed by TGA/DSC, DSC and ^{1}H NMR. The XRPD diffractograms for the unground and ground materials are shown in Fig. 9. This confirms the material is indeed Pattern 1, but there is still evidence of some extra peaks as shown in the region of 8.65° 2θ and 14.68° 2θ and the expansion in Fig. 10 illustrates this in finer detail.

Figure 9: *Transmission mode XRPD diffractogram of material from methanol pre and post grinding.*

Figure 10: *Expansion of transmission mode XRPD diffractogram of material from methanol pre and post grinding.*

Thermal analysis of these two samples showed no significant differences. For the unground material, TGA/DSC analysis showed no weight loss until decomposition above 330°C, with the corresponding DSC thermogram showing a single endothermic event with an onset at 314°C. The ground material showed a very similar thermal profile with no significant weight loss until gross decomposition started around 314°C with the DSC melt/decomposition onset occurring at 316°C. High accuracy DSC analysis using a standalone instrument provided similar DSC thermograms. The melt/decomposition onset temperature for the ground material being 315.6°C for the unground and 316.2°C for the ground material. While there were small differences observed, there was no evidence of a form change or a phase contaminant. The difference is attributed to the smaller particles size of the ground material having better contact with the DSC pan surface, giving more efficient, and thus, quicker heating of the sample. The DSC thermograms are shown in Fig. 11.

Figure 11: *Overlay of DSC thermograms of material from methanol pre (unground) and post grinding.*

The ^{1}H NMR of the two samples showed only small amounts of residual methanol, 0.08eq for both the unground and ground samples. The chemical integrity of ALZ-801 was unchanged.

The sample from THF-water was analyzed using TG/DSC, DSC and ^{1}H NMR and the analyses were repeated following a gentle grinding using a pestle and mortar. The ground solid was also analyzed by TG/DSC, DSC and ^{1}H NMR.

The XRPD diffractograms for the unground (black line) and ground (red line) materials are shown in Fig. 12. This data confirm the material is Pattern 1, but there is still evidence of some extra peaks as shown in the region of 8.96° 2θ and 18.11° 2θ and the expansion in Fig. 13 exemplifies this in finer detail.

Figure 12: *Transmission mode XRPD diffractogram of material from THF-water pre and post grinding.*

Figure 13: *Expansion of transmission mode XRPD diffractogram of material from THF-water pre (unground) and post grinding.*

Thermal analysis of these two samples showed no significant differences. The TGA/DSC analysis showed no weight loss until decomposition above 330°C, with the corresponding DSC thermogram showing a double endothermic event with an onset at 322°C. The ground material showed a very similar thermal profile with no significant weight loss until gross decomposition starting around 330°C and the DSC melt/decomposition onset at 323°C. More accurate DSC analysis using a standalone instrument provided similar DSC thermograms with the melt/decomposition onset temperature for the ground material being 316.1°C for the unground and 316.3°C for the ground material. There was no evidence of a form change, or a phase contaminant and the difference was not significant. The DSC thermograms are shown in Fig. 14.

Figure 14: *Overlay of DSC thermograms of material from THF-water pre and post grinding.*

Long term thermal cycling

The extra peaks observed post grinding may be the result of a phase impurity. Longer thermal cycling in solvent was evaluated to assess potential changes in the extra peaks observed. Following one week of thermal cycling between ambient and 40°C, extra peaks were still observed post grinding. This material was analyzed using 18 separate aliquots, and 8 showed extra peaks by transmission XRPD and 10 did not. Example XRPD diffractograms are shown in Fig. 15.

Figure 15: *Transmission mode XRPD diffractogram of ALZ-801 post extended slurrying in EtOH-water.*

The preferred orientation and extra peaks observed in multiple samples of ALZ-801 throughout this investigation led to the analysis of multiple samples of a single batch of API not only by transmission XRPD, but also by reflectance XRPD and by capillary XRPD. These were conducted to determine whether these slightly different techniques also resulted in the same issue. Material was analyzed by transmission mode XRPD 84 times and the same batch of material was ground gently and analyzed an additional 24 times for a total of 108 separate samples analyzed. Of these 108, 68 showed extra peaks that were not present in the reference XRPD diffractogram.

An example is shown in Fig. 16 and the rest of the diffractograms are available in the SI.

Figure 16: *Example transmission mode XRPD diffractograms from multiple analysis experiments.*

When the same batch of material was analyzed by reflectance mode 15 samples of ground material were assessed, and none showed any evidence of extra peaks. Two XRPD diffractograms are shown in Fig. 17.

Figure 17: *Example reflectance mode XRPD diffractograms from multiple analysis experiments.*

Concurrently capillary XRPD was utilized with a single crystal X-Ray diffractometer. The diffractograms obtained were all consistent with each other, none showing any extra peaks (see Fig. 18) but also consistent with the predicted XRPD obtained from the single crystal structure as shown in Fig. 19.

Figure 18: *Example capillary mode XRPD diffractograms from multiple analysis experiments.*

Figure 19: *Capillary mode XRPD diffractogram and predicted XRPD diffractogram from SC-XRD.*

The structure obtained of ALZ-801 demonstrated a dense crystal structure with hydrogen bonds satisfied with no evidence that a more stable form might be possible such as voids or unsatisfied hydrogen bonds (Fig. 20).

Figure 20: *The two-dimensional hydrogen bonding network structure of ALZ-801.*

Conclusions

The present structural and analytical studies demonstrate that ALZ-801 occurs solely as a single polymorphic crystal form with excellent in vivo pharmaceutical properties [6] and promising efficacy (8,9) The API is highly crystalline, thermally stable, and exhibits excellent aqueous solubility. Interestingly, ALZ-801 displays potential artifacts in the transmission mode XRPD analysis which are not observed in reflectance or capillary mode XRPD. Therefore, while only a single high solubility crystalline form of ALZ-801 is observed, the risk of a change in solid form affecting the delivery of this potential new disease modifying therapy for Alzheimer's disease is negligible.

In summary, the favorable pharmacodynamic properties and efficacy in Early AD subjects (8,9) and physicochemical characteristics properties of ALZ-801 support the development of oral ALZ-801 265mg BID dose regimen as a potential oral disease-modifying agent for treatment of AD.

Declarations

Funding support: The analyses in this report were supported by Alzheon, Inc.

Conflicts of interest: John A. Hey, Jean F. Schaefer, and Martin Tolar are employees of Alzheon, Inc. John Amedio, serves as a consultant to Alzheon, Inc. All authors own Alzheon stocks and/or stock options.

David Pearson is an employee of Sygnature Discovery.

Availability of data and material: The ALZ-801 data are proprietary to Alzheon Inc.

Code availability: Not applicable.

Author's contributions: DP wrote the article in collaboration with JA, JFS; SA, JAH and MT. DP designed and conducted the ALZ-801 laboratory work. All authors have read and approved the final submitted manuscript and agree to be accountable for the work.

References

1. Tolar M, Hey JA, Power A, Abushakra S (2024) The Single Toxin Origin of Alzheimer's Disease and Other Neurodegenerative Disorders Enables Targeted Approach to Treatment and Prevention. Int J Mol Sci Feb 27(5):2727
2. Tolar M, Hey J, Power A, Abushakra S (2021) Neurotoxic soluble amyloid oligomers drive Alzheimer's pathogenesis and represent a clinically validated target for slowing disease progression. Int J Mol Sci 22:6355. 10.3390/ijms22126355
3. Knopman DS, Amieva H, Petersen RC, Chételat G, Holtzman DM, Hyman BT, Nixon RA, Jones DT (2021) Alzheimer disease. Nat Rev Dis Primers May 13(1):7
4. Tolar M, Abushakra S, Sabbagh M (2020) The path forward in Alzheimer's disease therapeutics: Reevaluating the amyloid cascade hypothesis. Alzheimers Dement 16:1553–1560
5. Gervais F, Paquette J, Morissette C et al (2007) Targeting soluble Abeta peptide with tramiprosate for the treatment of brain amyloidosis. Neurobiol Aging 28:537–547
6. Kocis P, Tolar M, Yu J et al (2017) Elucidating the Aβ42 Anti-Aggregation Mechanism of Action of Tramiprosate in Alzheimer's Disease: Integrating Molecular Analytical Methods, Pharmacokinetic and Clinical Data. CNS Drugs Jun; 31(6):495–509
7. Hey JA, Kocis P, Hort J et al (2018) Discovery and identification of an endogenous metabolite of tramiprosate and its prodrug ALZ-801 that inhibits beta amyloid oligomer formation in the human brain. CNS Drugs 32:849–861
8. Liang C, Savinov SN, Fejzo J et al (2019) Modulation of amyloid-β42 conformation by small molecules through non-specific binding. J Chem Theor Comput 15:5169–5174
9. Hey JA, Yu JY, Abushakra S et al (2024) Analysis of Cerebrospinal Fluid, Plasma β-Amyloid Biomarkers, and Cognition from a 2-Year Phase 2 Trial Evaluating Oral ALZ-801/Valiltramiprosate in APOE4 Carriers with Early Alzheimer's Disease Using Quantitative Systems Pharmacology Model. Drugs https://doi.org/10.1007/s40265-024-02068-7
10. Hey JA, Abushakra S, Blennow K et al (2024) Effects of Oral ALZ-801/Valiltramiprosate on Plasma Biomarkers, Brain Hippocampal Volume, and Cognition: Results of 2-Year Single-Arm, Open-Label, Phase 2 Trial in APOE4 Carriers with Early Alzheimer's Disease. Drugs. https://doi.org/10.1007/s40265-024-02067-8

11. Abushakra S, Hey J, Blennow K K, et al (2022) Effects of oral ALZ-801, an amyloid oligomer inhibitor, on plasma biomarkers in APOE4 carriers with Early Alzheimer's disease: results of six-month interim analysis from a phase 2 biomarker study. Alzheimers Dement 18:e069141
12. Abushakra S, Porsteinsson A, Vellas B et al (2016) Clinical benefits of tramiprosate in Alzheimer's disease are associated with higher number of APOE4 alleles: the APOE4 gene-dose effect. J Prev Alzheimers Dis 3:219–228
13. Abushakra S, Porsteinsson A, Scheltens P et al (2017) Clinical effects of tramiprosate in APOE4/4 homozygous patients with mild Alzheimer's disease suggest disease modification potential. J Prev Alzheimers Dis 4:149–156
14. Li M, Xu W, Yongchao Su (2021) Solid-state NMR spectroscopy in pharmaceutical sciences. TRAC Trends Anal Chem 135:116152
15. Le Pevelen DD, Tranter GE (2017) FT-IR and Raman Spectroscopies, Polymorphism Applications, Editor(s): John C. Lindon, George E. Tranter, David W. Koppenaal, Encyclopedia of Spectroscopy and Spectrometry (Third Edition), Academic Press, Pages 750–761, ISBN 9780128032244
16. Blanco M, Bautista M, Alcalà M (2008) API Determination by NIR Spectroscopy Across Pharmaceutical Production Process. AAPS PharmSciTech 9:1130–1135
17. Putnis A (1992) *Introduction to Mineral Sciences*. Cambridge, UK: Cambridge University Press. Chapter 3 (pp. 41–80)

Figures

Figure 1

Chemical structure of ALZ-801 and tramiprosate

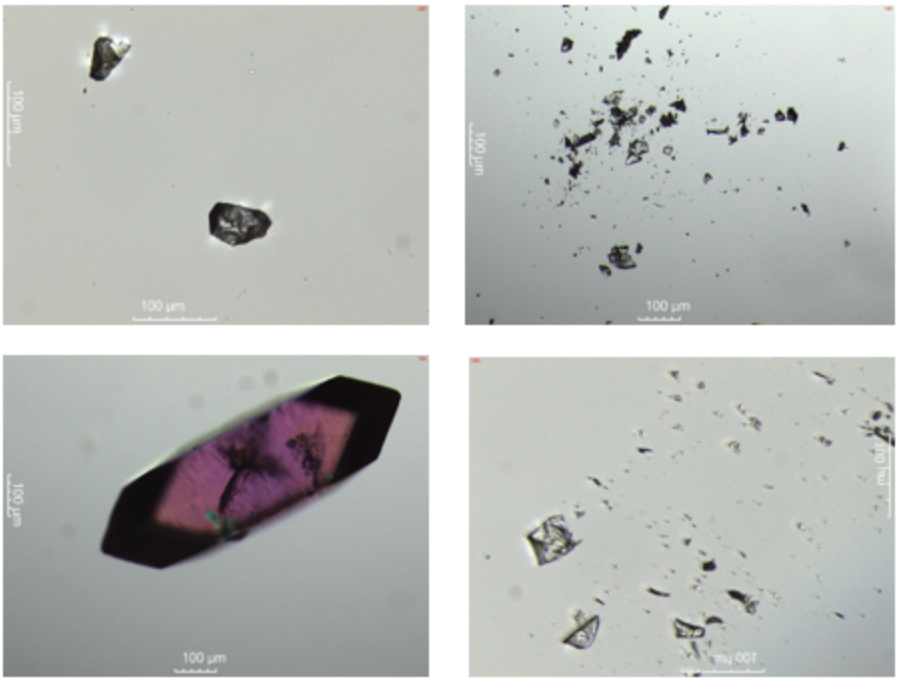

Figure 2

Phase light microscopy image of ALZ-801 crystal pattern 1 (single polymorph). ALZ-801 crystals occur in diverse ranges of morphologies, i.e., tetrahedron, bladed, needles, dodecahedron, slices, prismatic and tabular forms.

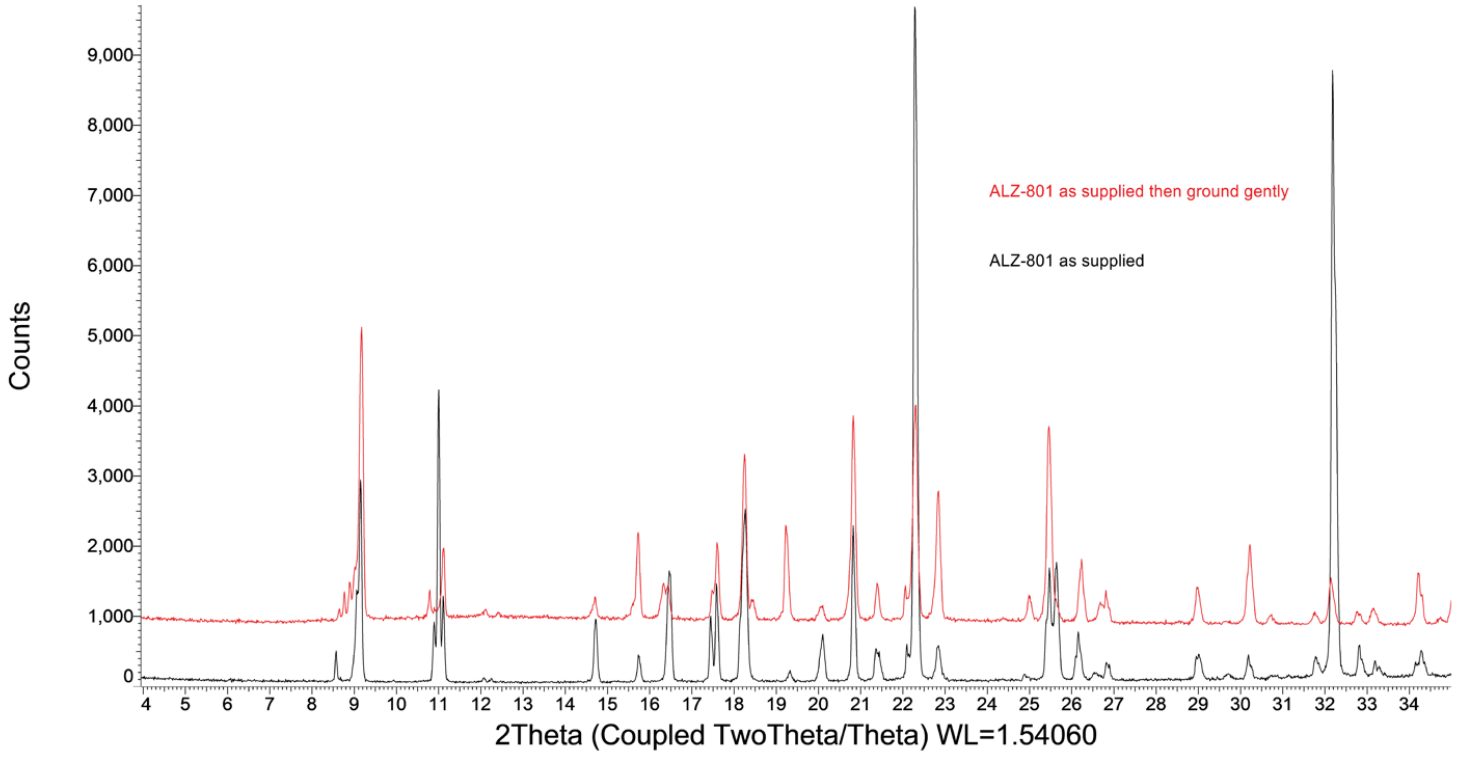

Figure 3

Transmission mode XRPD Diffractogram of ALZ-801 as received and after grinding.

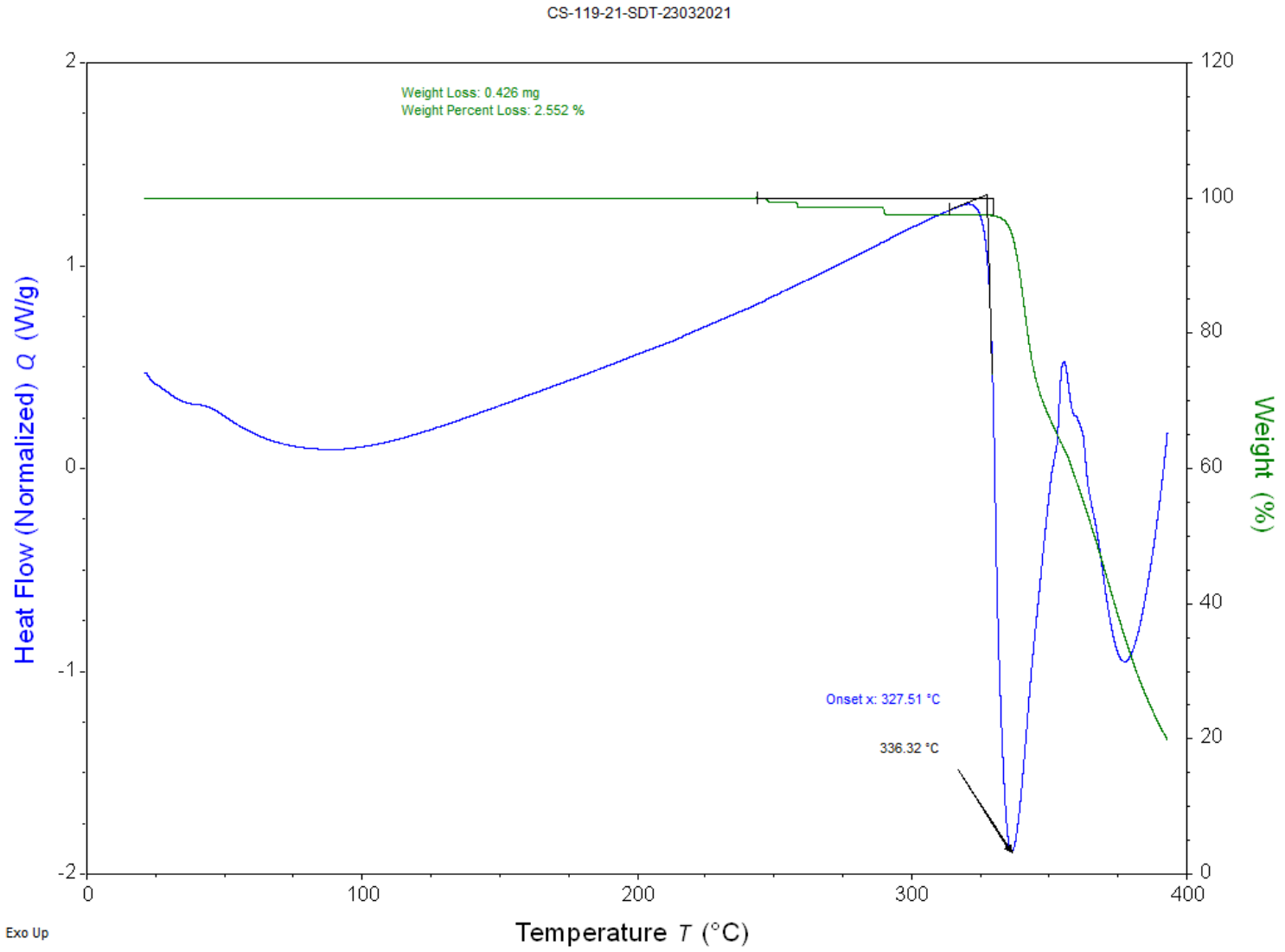

Figure 4

TGA/DSC Thermogram of ALZ-801 as received.

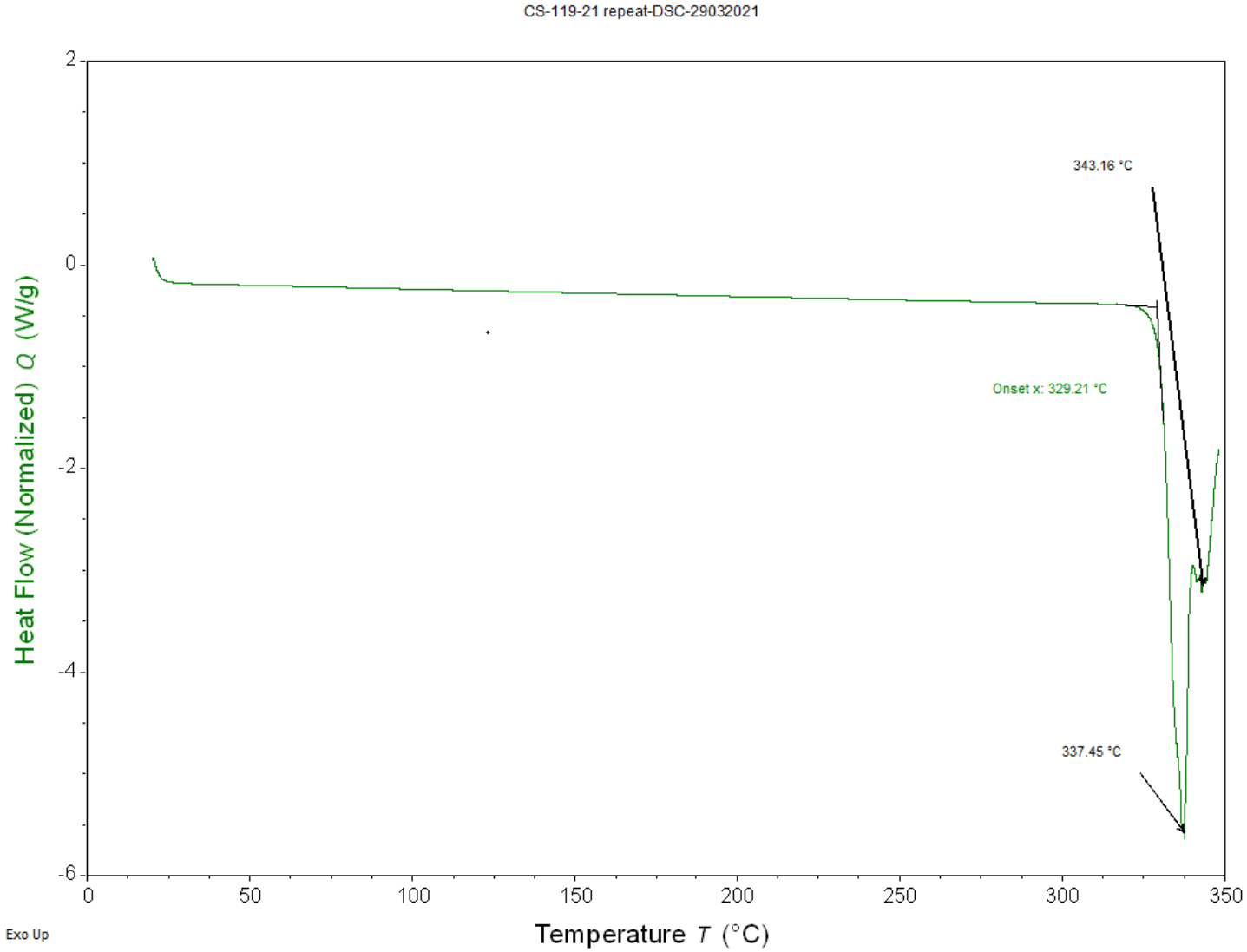

Figure 5

DSC Thermogram of ALZ-801 as received.

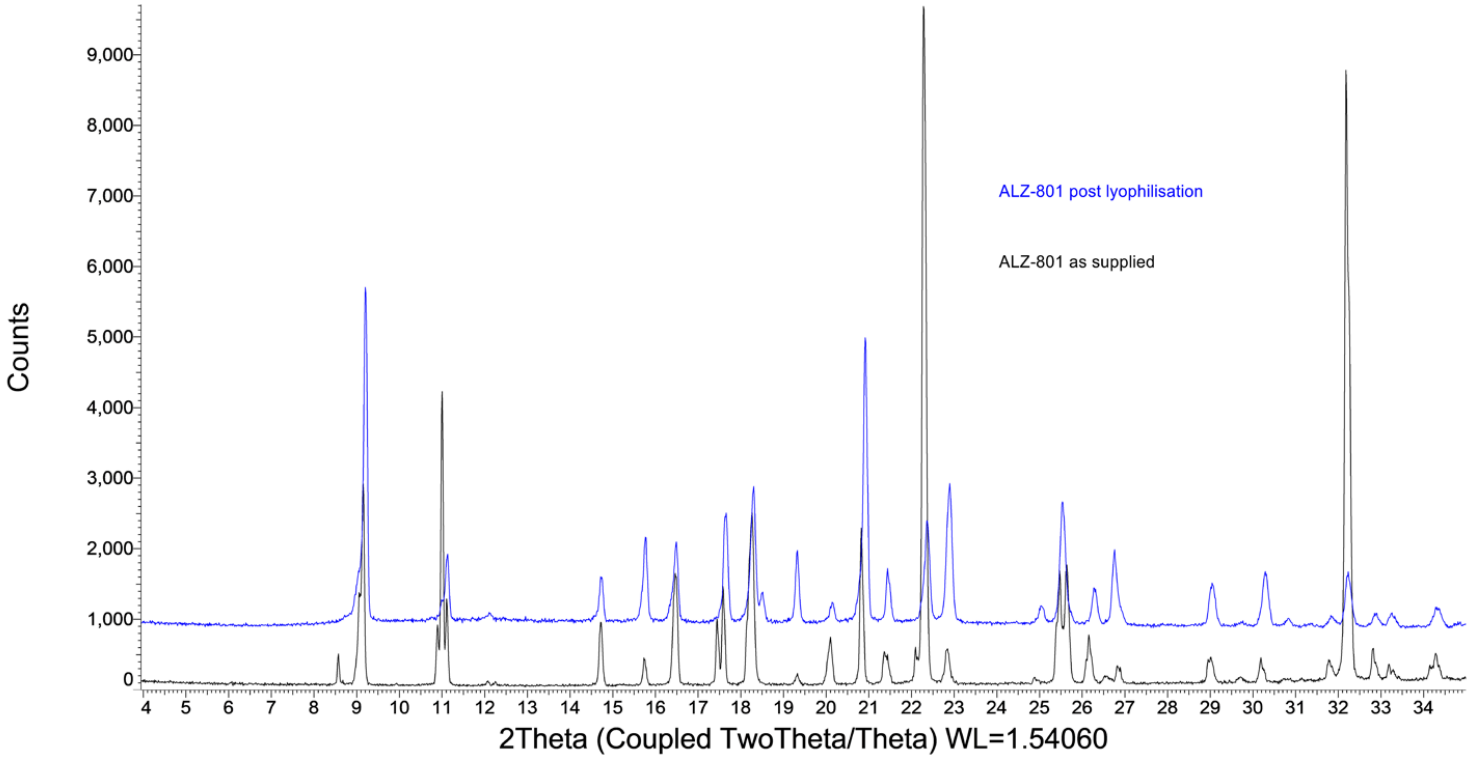

Figure 6

Transmission XRPD Diffractogram of ALZ-801 pre and post lyophilization.

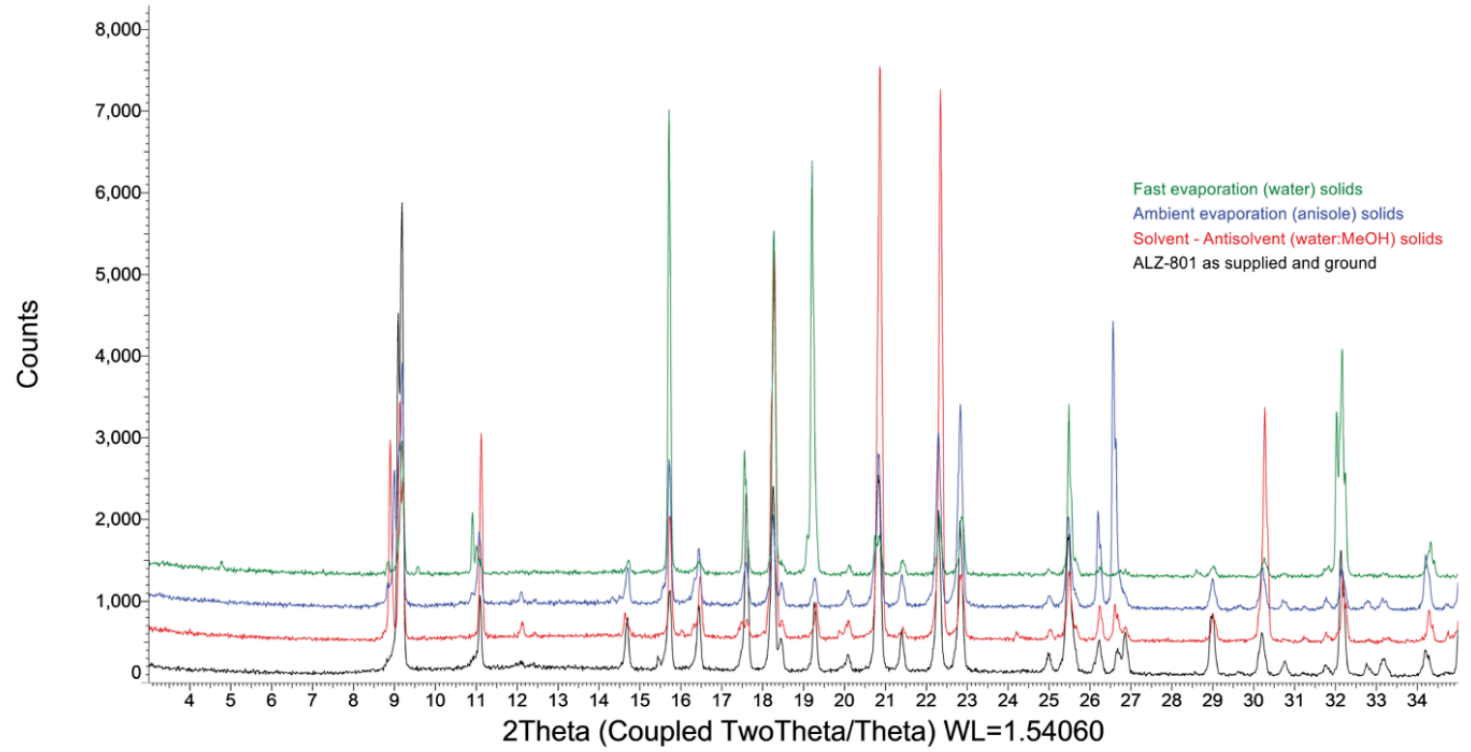

Figure 7

Transmission mode XRPD diffractograms from selected experiments.

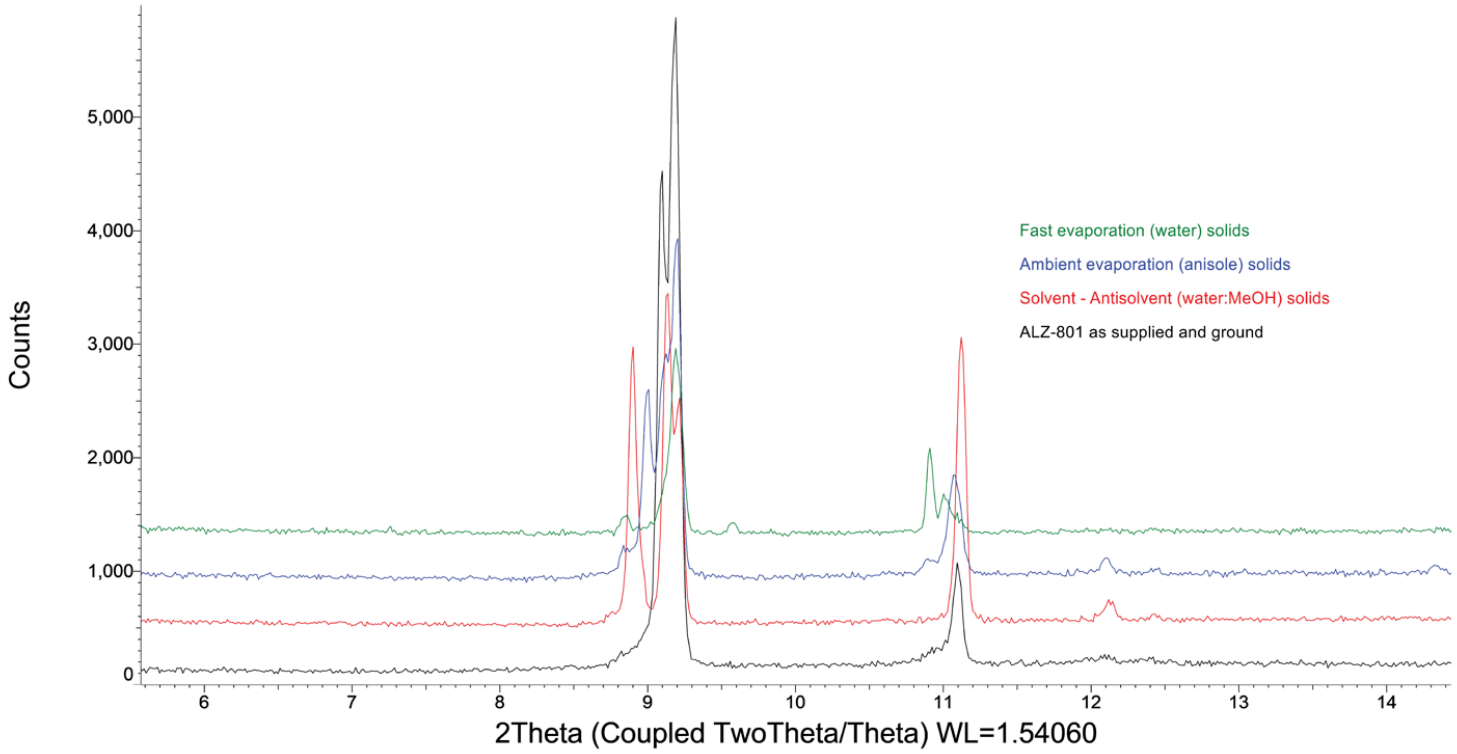

Figure 8

Expansion of transmission mode XRPD diffractograms from selected experiments.

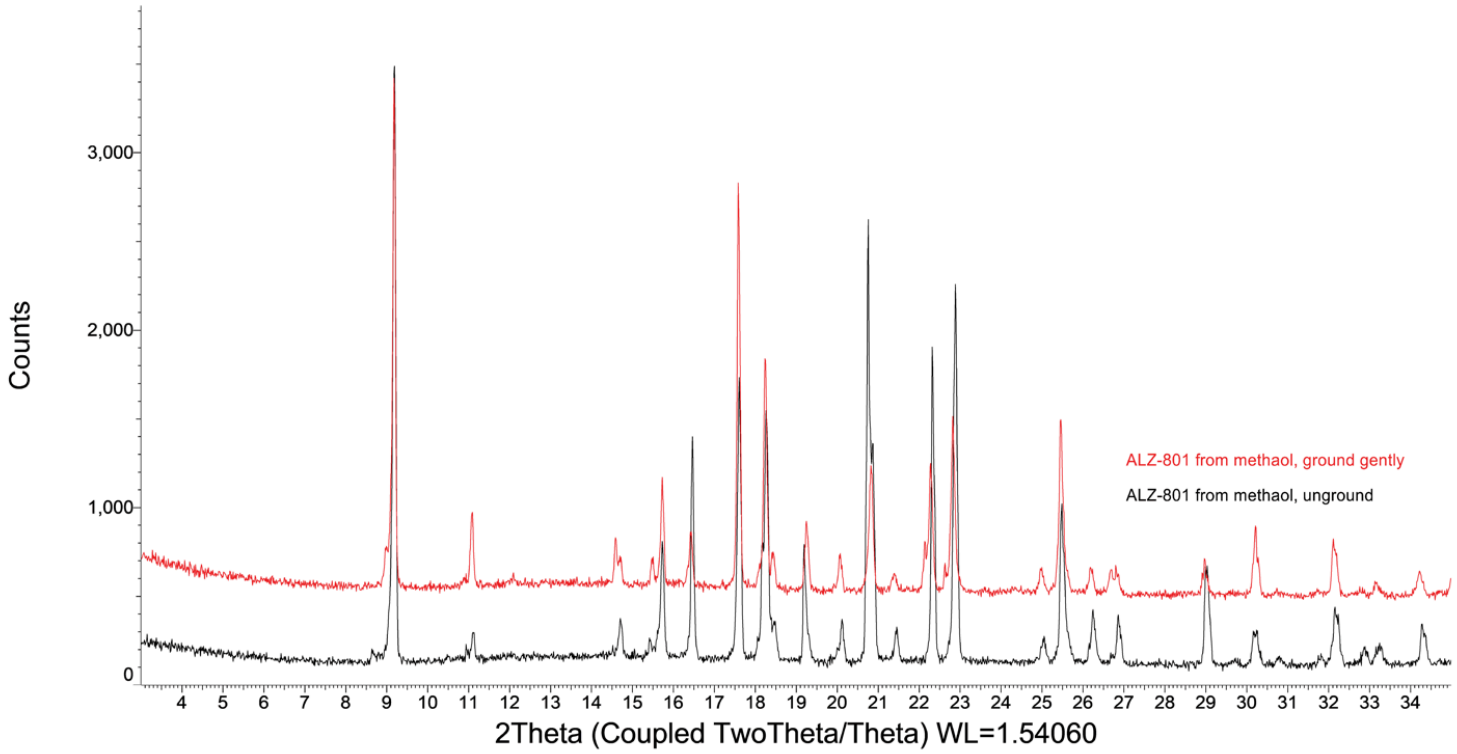

Figure 9

Transmission mode XRPD diffractogram of material from methanol pre and post grinding.

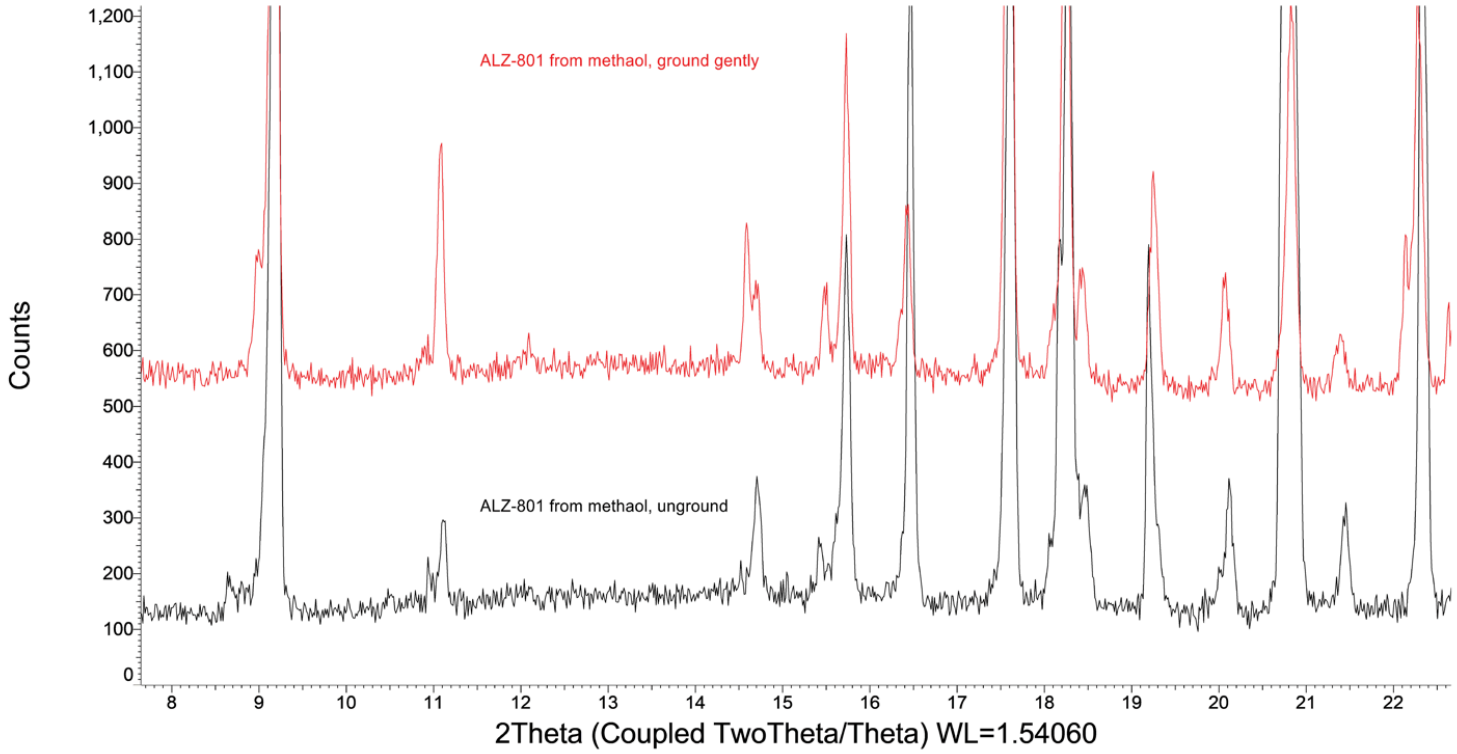

Figure 10

Expansion of transmission mode XRPD diffractogram of material from methanol pre and post grinding.

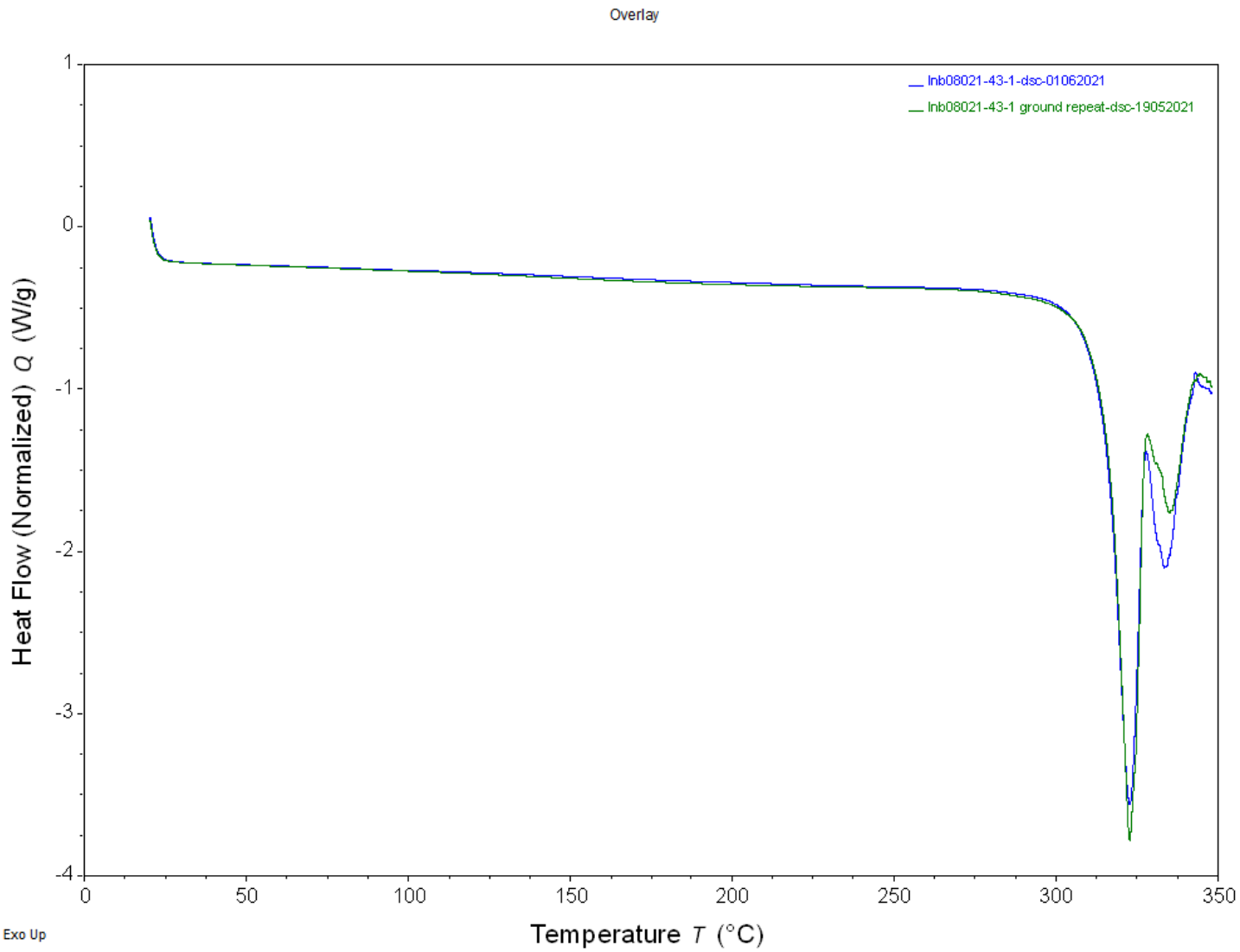

Figure 11

Overlay of DSC thermograms of material from methanol pre (unground) and post grinding.

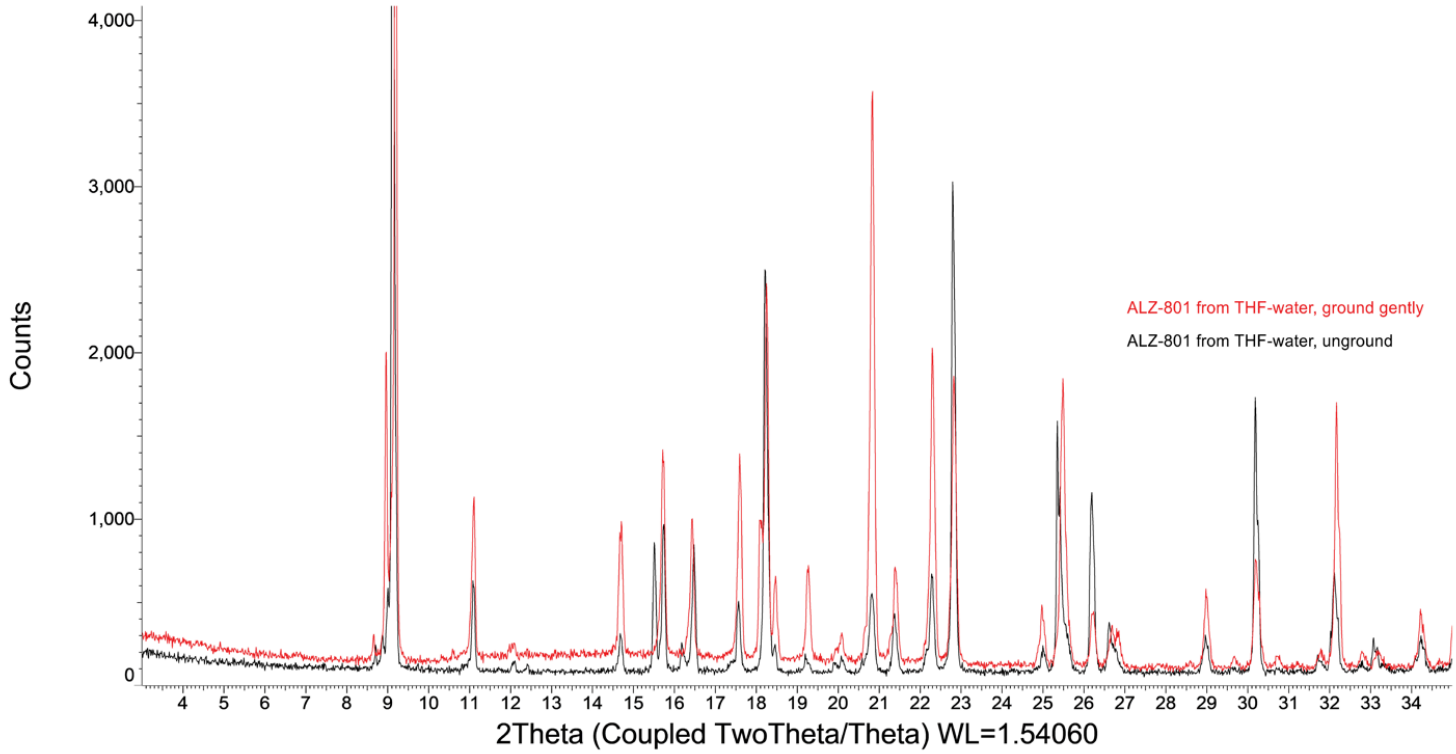

Figure 12

Transmission mode XRPD diffractogram of material from THF-water pre and post grinding.

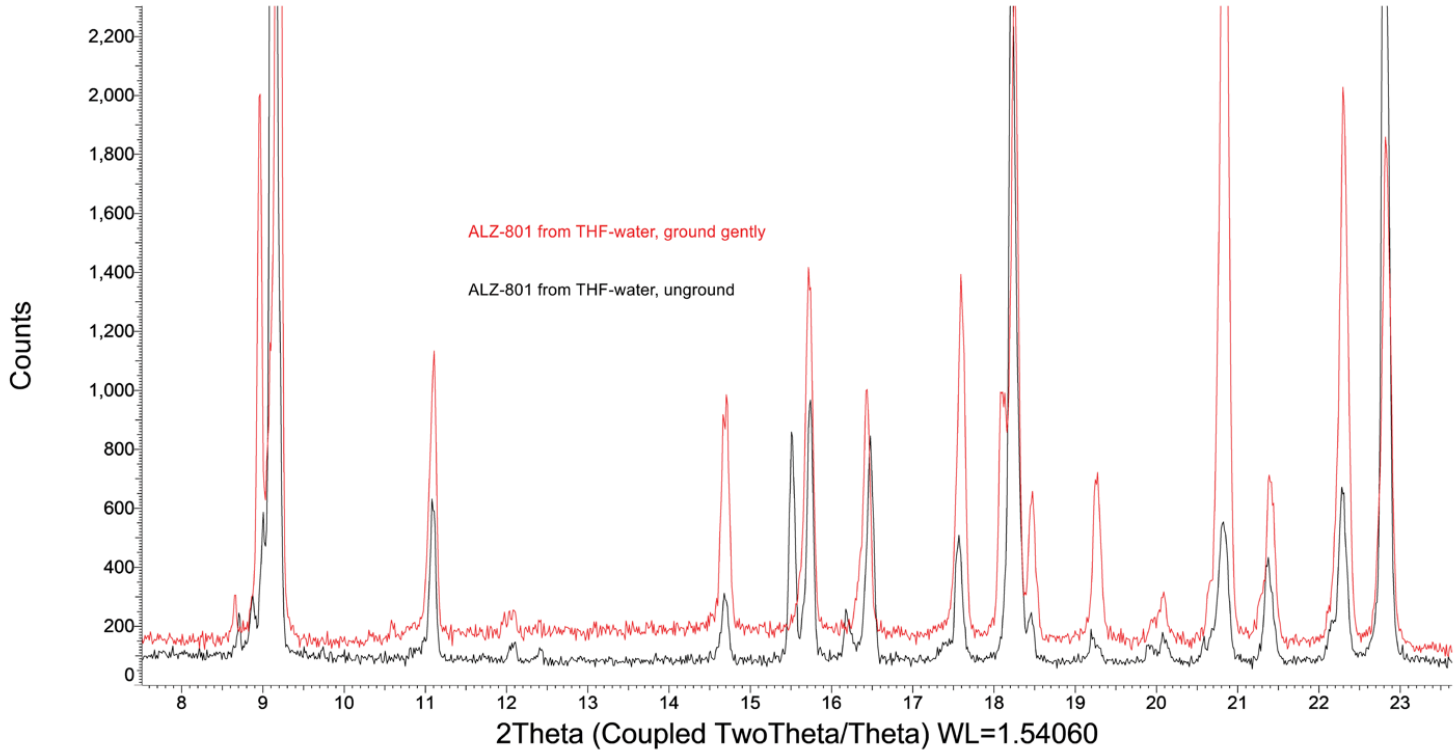

Figure 13

Expansion of transmission mode XRPD diffractogram of material from THF-water pre (unground) and post grinding.

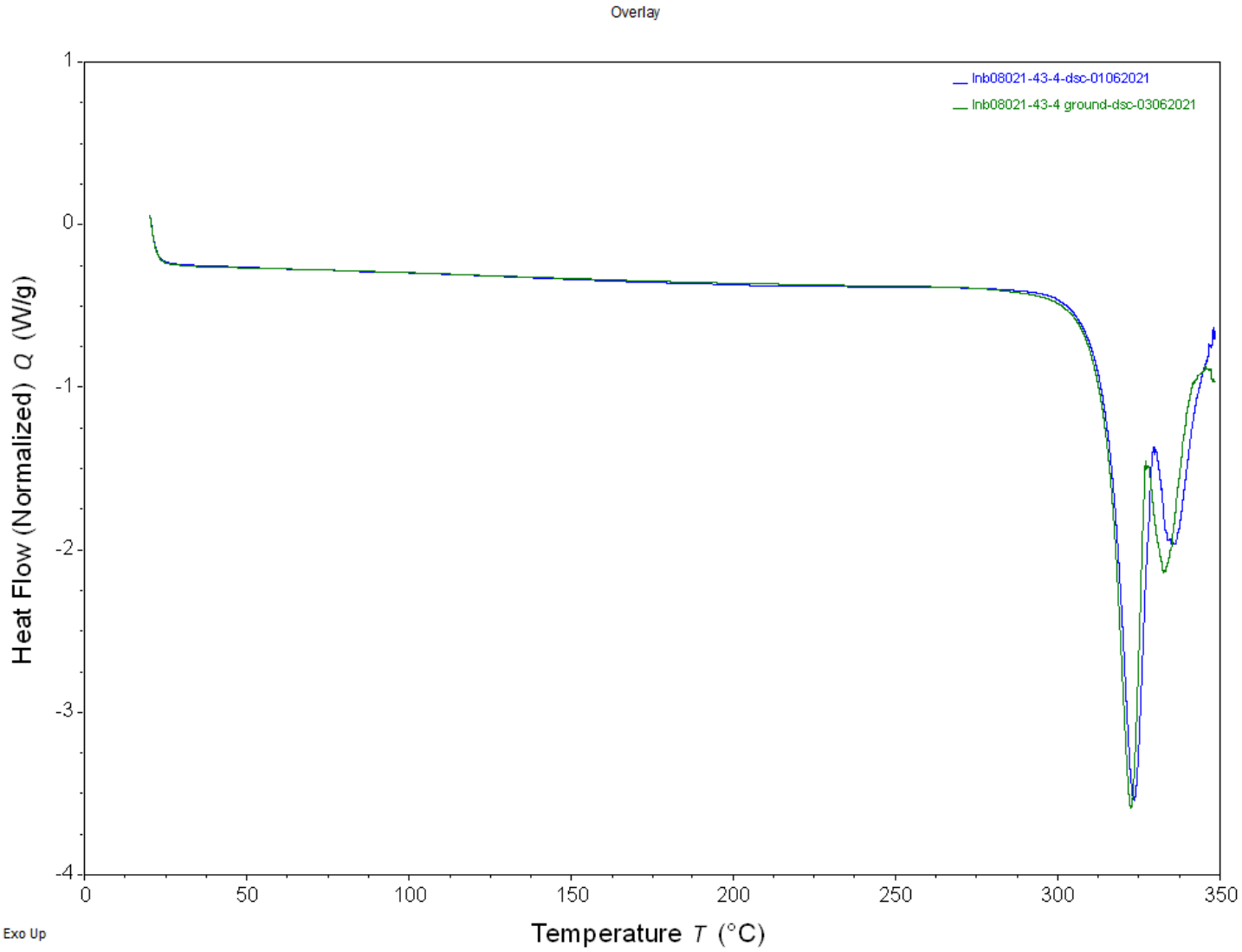

Figure 14

Overlay of DSC thermograms of material from THF-water pre and post grinding.

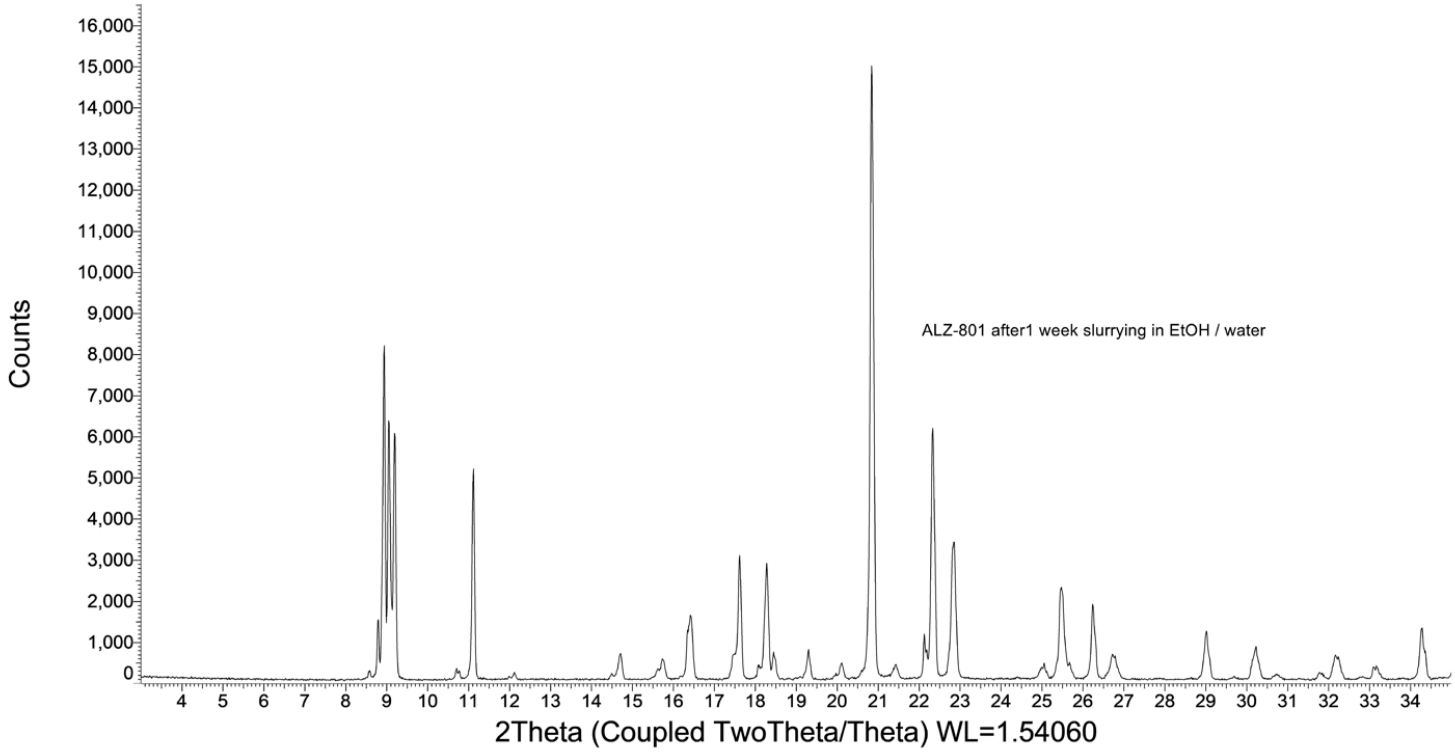

Figure 15

Transmission mode XRPD diffractogram of ALZ-801 post extended slurrying in EtOH-water.

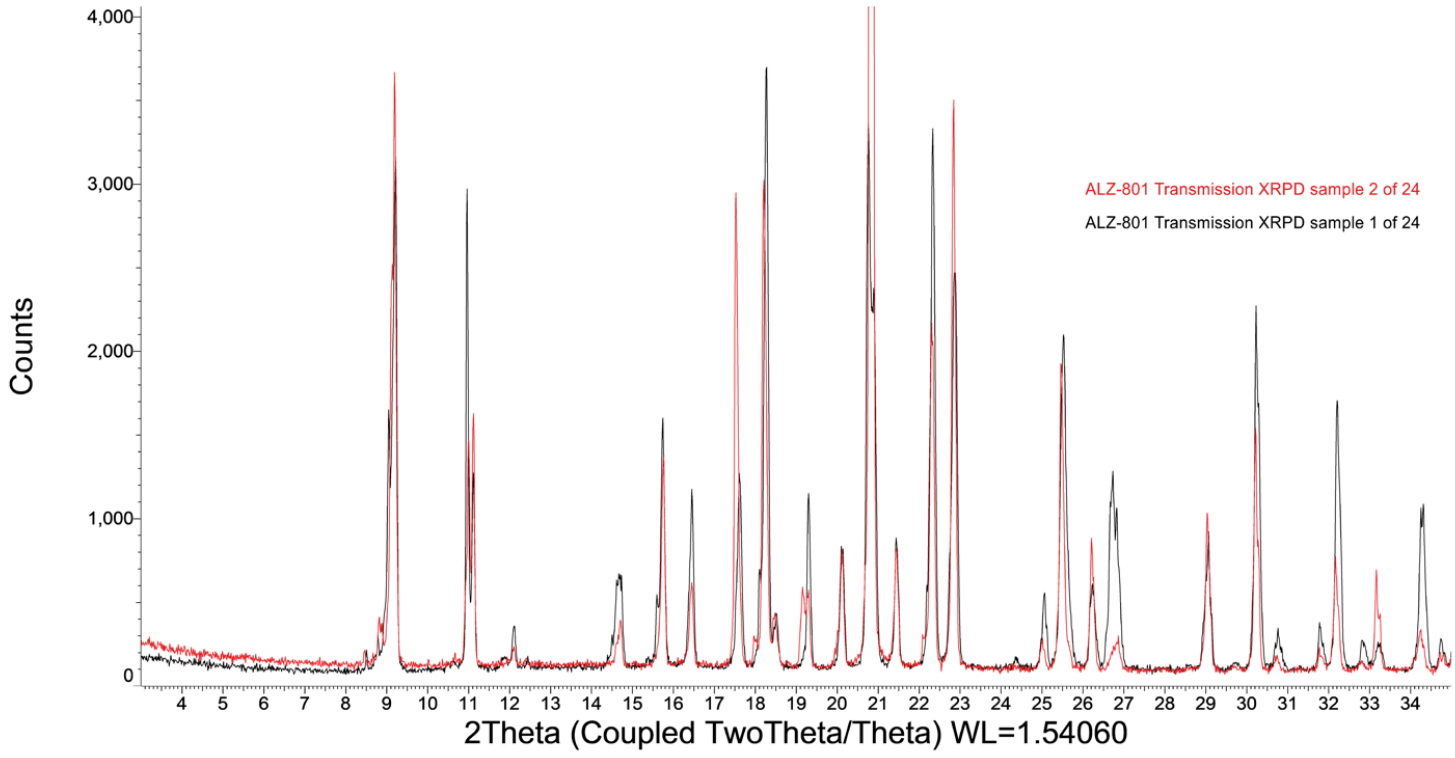

Figure 16

Example transmission mode XRPD diffractograms from multiple analysis experiments.

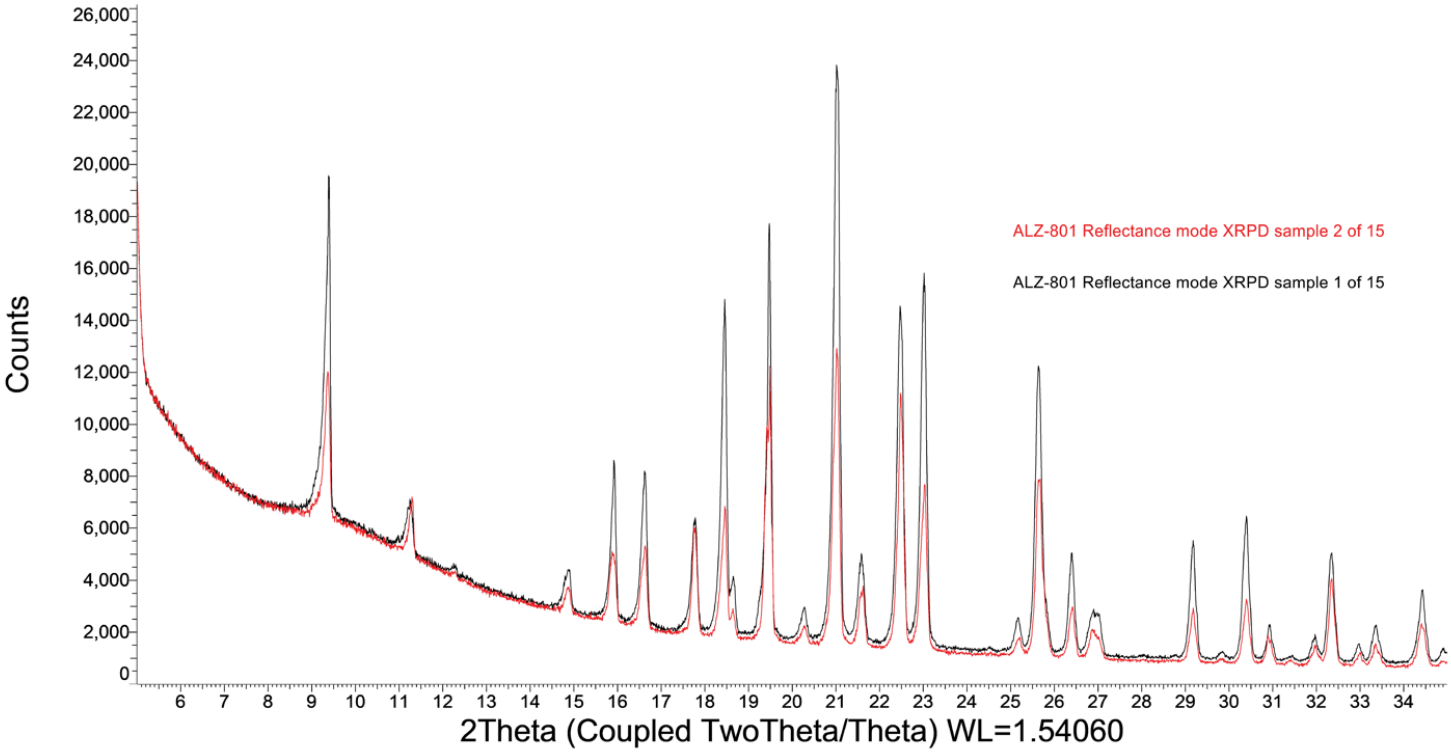

Figure 17

Example reflectance mode XRPD diffractograms from multiple analysis experiments.

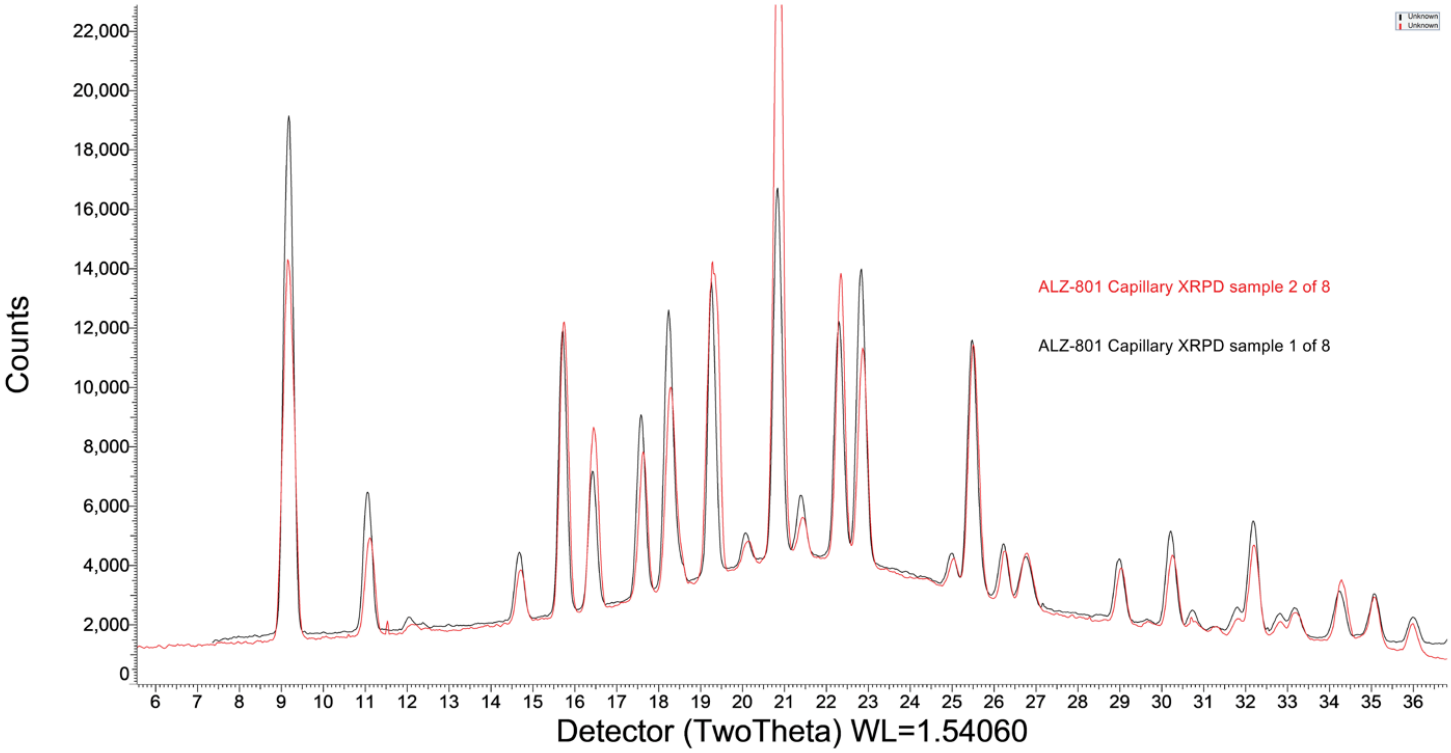

Figure 18

Example capillary mode XRPD diffractograms from multiple analysis experiments.

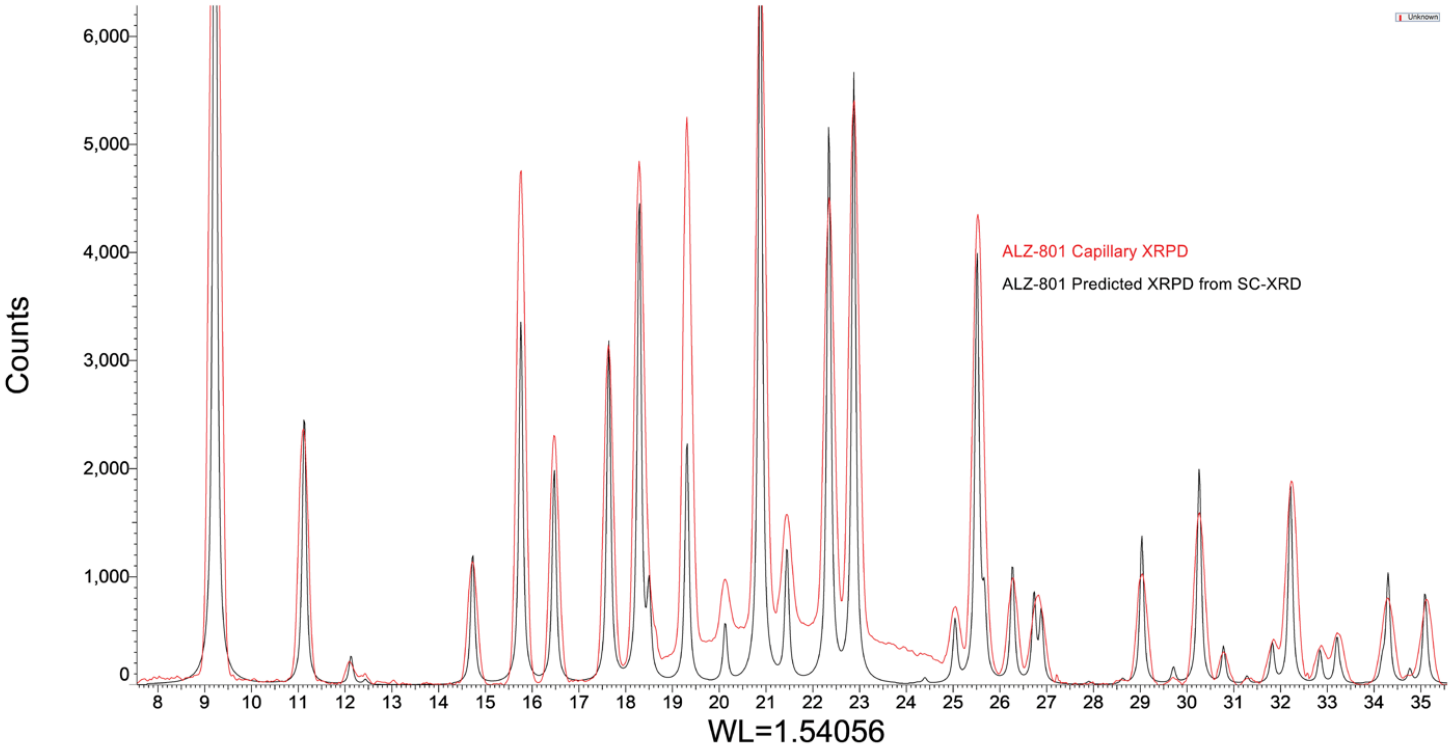

Figure 19

Capillary mode XRPD diffractogram and predicted XRPD diffractogram from SC-XRD.

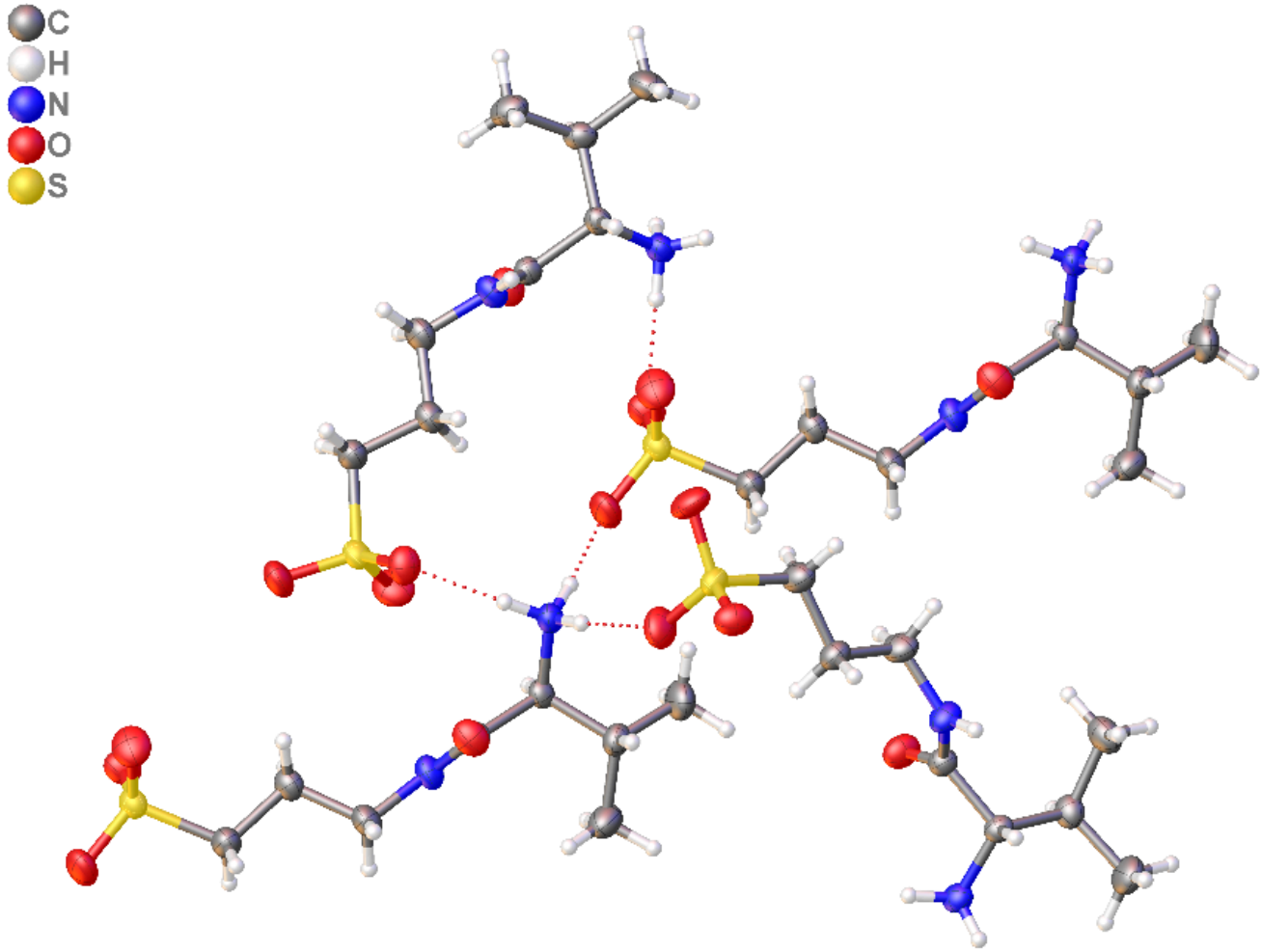

Figure 20

The two-dimensional hydrogen bonding network structure of ALZ-801.

Supplementary Files

This is a list of supplementary files associated with this preprint. Click to download.

- AbstractIndex.docx